The Influence of Debye Length on the C–V Measurement of Doping Profiles

WALTER C. JOHNSON, FELLOW, IEEE, AND PETER T. PANOUSIS, MEMBER, IEEE

Abstract—The doping profile of a semiconductor is given only approximately by the conventional analysis of C–V measurements. The present study employs computer simulation of semiconductors with one-sided doping profiles that consist of high and low doped sections joined by steps and linear ramps. The computation yields the apparent doping profile that would be obtained by the conventional use of C–V data, and this result is compared with the actual profile, with the majority-carrier distribution, and with the outcome of a correction previously proposed in the literature.

The results show that a step in the profile cannot be resolved satisfactorily to less than several Debye lengths corresponding to the doping on the high side of the profile. A ramp cannot be distinguished accurately from a step unless its width is appreciably greater than a Debye length. Furthermore, the apparent doping profile is not identical with the majority-carrier distribution with contacts far away, as has been suggested, and the discrepancy is shown to depend on the side from which depletion is done.

I. Introduction

DOPING profiles in semiconductors are commonly determined by a differential capacitance technique [1]. A degenerately doped p-n junction or a metallic Schottky barrier is formed at the surface of the semiconductor. This junction is placed in reverse bias, and the capacitance of the transition layer is measured as a function of the bias voltage. The analysis of the capacitance versus bias voltage relationship is conveniently done using the depletion-layer approximation in which the semiconductor is assumed to be divided into two distinct regions: a layer that is entirely depleted of charge carriers, and an interior region of perfect charge neutrality. The foregoing is equivalent to assuming zero value for the Debye screening length in the vicinity of the assumed edge of the space-charge layer. If the doping profile has large gradients and if spatial resolution is attempted on the order of a few Debye lengths in the vicinity of these gradients, the assumption of a zero Debye length can produce serious errors in the calculation of the doping profile from the C–V data. Unfortunately, a more accurate interpretation of C–V data is considerably more difficult because of the nonlinear relations that are involved. This paper states briefly the conventional interpretation, considers the physical basis for a more accurate interpretation, and reviews recent hypotheses regarding the role of the free charge carriers; then, using computer simulation for step and ramp doping profiles, shows the effect of the Debye length on the interpretation of C–V data.

Manuscript received April 12, 1971.

W. C. Johnson is with Princeton University, Princeton, N. J., and Bell Telephone Laboratories, Inc., Murray Hill, N. J. 07974.

P. T. Panousis is with Bell Telephone Laboratories, Inc., Murray Hill, N. J. 07974.

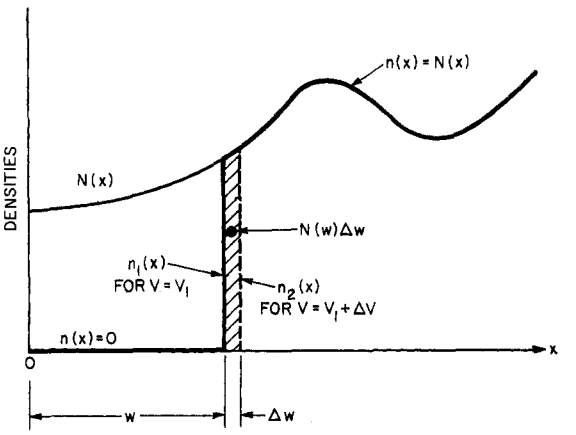

Fig. 1. Illustrating the usual assumption of a sharp-edged distribution of $n(x)$. The shaded ordinates represent the increment $\Delta n(x) = n_1(x) - n_2(x)$.

II. Conventional Interpretation of C–V Data

In the usual analysis of C–V data, it is assumed that the transition region has a sharply defined edge in the manner illustrated in Fig. 1. The notation is as follows.

- x Distance measured from the contact into the semiconductor.
- w Width of the depletion layer.
- $N(x)$ Net density of ionized impurity atoms.
- $n(x)$ Density of majority carriers.

Specifically, the usual assumptions are that $n(x) = 0$ for $0 < x < w$, and that for $x > w$ the semiconductor is electrically neutral with $n(x) = N(x)$. Minority carriers are neglected throughout.

Fig. 1 shows the assumed sharp edge of $n(x)$ for two bias voltages that differ by a small increment ΔV, thus producing an increment in width Δw. In effect, the majority-carrier increment $\Delta n(x) = n_1(x) - n_2(x)$, shown shaded in Fig. 1, provides a sample of the doping profile $N(x)$ at $x = w$. The charge removed from the edge of the depletion layer is $\Delta Q = qN(w)\Delta w$ C/unit area, where q is the magnitude of the electronic charge. The charge ΔQ is passed through the external circuit, while within the depletion layer there is produced an increment of electric field $\Delta E = \Delta Q/\epsilon$ where ϵ is the dielectric permittivity of the semiconductor. The increment of voltage is given by $\Delta V = w\Delta E = qN(w)w\Delta w/\epsilon$, and the capacitance measured by external instruments is $C = \Delta Q/\Delta V = \epsilon/w$ F/unit area. The latter expression can be written as $w = \epsilon C^{-1}$. Thus $\Delta w = -\epsilon C^{-2}\Delta C$, and we can write the increment of voltage as ΔV

$= qN(w) \cdot (-\epsilon C^{-2}\Delta C)(\epsilon C^{-1})/\epsilon$, from which we obtain the following conventional formulas:

$$N(w) = -\frac{C^3}{q\epsilon}(dC/dV)^{-1} \tag{1}$$

where

$$w = \epsilon/C. \tag{2}$$

III. The Effect of a Nonzero Debye Length—Physical Discussion

It is well known that the use of (1) and (2) provides only an approximation to the actual doping profile. The zero value of current that is tacitly assumed requires a balance between diffusion and drift currents, and this in turn requires an electric field wherever dn/dx is different from zero. In particular, the diffusion of majority carriers prevents $n(x)$ from having the sharp step that was envisioned in Fig. 1, and therefore the increment $\Delta n(x)$ does not provide a precise sample of $N(x)$ at $x = w$.

The true situation, which will be detailed in more quantitative fashion in Section V, is illustrated in Fig. 2, which is drawn for a high–low step profile. The graph labeled $n_0(x)$ represents the distribution of majority carriers that would be obtained in thermal equilibrium if both contacts were infinitely far away. The natural measure of distance here is the extrinsic Debye screening length:

$$\lambda = \sqrt{\frac{kT\epsilon}{q^2N}} \tag{3}$$

where k is the Boltzmann constant, T is the absolute temperature, and N is the local density of doping. On the horizontal axis of Fig. 2(a) are shown the two Debye lengths, λ_{low} and λ_{high}, that correspond to the intensities of doping, N_{low} and N_{high}, on the two sides of the step. It is only at a distance of several Debye lengths from the step that the carrier density $n_0(x)$ approaches closely to the density of doping, $N(x)$.

The solid graph labeled $n_1(x)$ in Fig. 2(a) represents the general form of the majority carrier distribution that is obtained if a rectifying contact is placed on the semiconductor at the left and is reverse biased. The region near the contact is essentially depleted of charge carriers, while far to the right $n_1(x)$ approaches $N(x)$. The transition between these two extremes depends on the space-charge distribution $q[N(x) - n_1(x)]$ which produces an electric field $E(x)$ such that at every point there exists a balance between the drift current $q\mu n(x)E(x)$ and the diffusion current $qD\, dn(x)/dx$. As is shown in Section V, the principal portion of the transition from depletion to space-charge neutrality occupies several Debye lengths.

If the reverse bias voltage is increased by an increment ΔV, there results a new majority-carrier distribution such as the one shown by the dashed curve labeled $n_2(x)$ in Fig. 2(a). The shaded ordinates, which are replotted in the lower graph of Fig. 2(a), represent the majority-carrier increment $\Delta n(x) = n_1(x) - n_2(x)$. This increment is spread out over several Debye lengths and clearly does not sample $N(x)$ in the manner that was visualized in Fig. 1. The capacitance measured by an external instrument does not define the width of the space-charge layer to better than a few Debye lengths, and the variation of capacitance with bias voltage can resolve changes in $N(x)$ only to about this degree of accuracy. For a relative dielectric constant of 12 and a net doping density of $N = 10^{15}$ cm^{-3}, we have $\lambda = 0.13$ μm at $T = 300$°K. Therefore the errors will be of concern only if the semiconductor is doped lightly or if one is attempting to resolve the profiles of very thin doped layers such as those that can be produced by ion implantation.

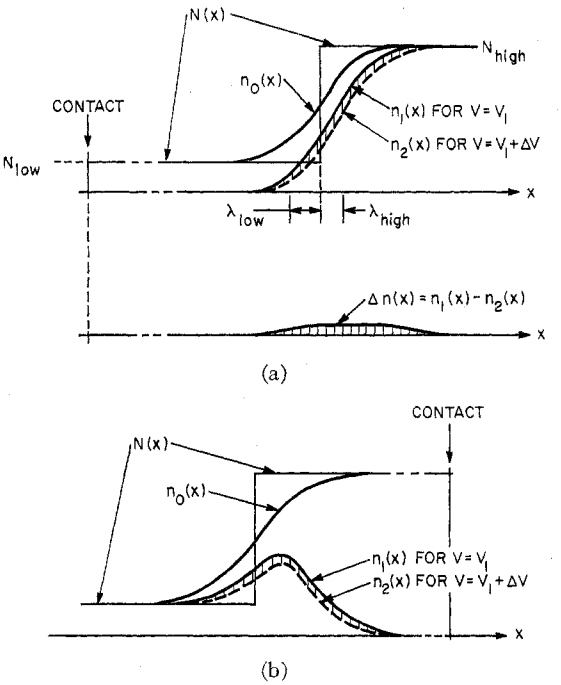

Fig. 2. Actual distributions of majority carriers for a step-function doping profile, and the increment $\Delta n(x) = n_1(x) - n_2(x)$ produced by an increment in bias voltage.

$\lambda_{low} = \sqrt{kT\epsilon/q^2N_{low}}$; $\lambda_{high} = \sqrt{kT\epsilon/q^2N_{high}}$.

(a) Depletion from low side. (b) Depletion from high side.

The calculation of $n(x)$ for a given doping function $N(x)$ and for a given bias voltage V requires the solution of a boundary-value problem involving nonlinear differential equations (see the Appendix). Numerical solution by iteration is feasible, however, on a large-scale digital computer, and from the results one can predict the capacitance C as a function of V for a given doping profile. On the other hand, the converse problem of computing $N(x)$ from the dependence of C on V is intractable, and it appears that one must be content with approximations. The interpretation of the approximate results may be aided, however, by insight gained

from analyses of the $C-V$ relationships for various types of doping profiles.

A further consideration should now be mentioned. Whereas Fig. 2(a) showed a high–low step profile with depletion done from a contact on the low side, Fig. 2(b) shows the results with an identical profile but with depletion done from a contact on the high side. The thermal-equilibrium distribution of majority carriers with contacts far away, $n_0(x)$, would of course be the same in both cases. With the contacts in place and with bias voltage applied, however, the results are quite different, and the carrier distributions $n_1(x)$ and $n_2(x)$ are not at all the same in Fig. 2(a) and 2(b). The results of capacitance measurements, therefore, are expected to be different for depletion done from contacts on opposite sides, and from this one can reason that such measurements cannot yield precise information regarding either $N(x)$ or $n_0(x)$. The foregoing conclusions are confirmed by the results given in Section V.

IV. Discussion of Some Recent Hypotheses

The use of thin doped layers and of doping profiles with large gradients has recently stimulated efforts to formulate a relation between $N(x)$ and the $C-V$ data that would give an improved estimate of $N(x)$ and still be reasonably easy to use. A valuable contribution in this direction has been made by Kennedy, Murley, and Kleinfelder (KMK) [2], who have pointed out the central role of the free majority carriers in the $C-V$ relationship and have proposed that formula (1), instead of yielding the doping profile, gives the distribution of majority carriers with contacts far away [$n_0(x)$ in the present notation]. Thus, they would replace (1) by

$$n_0(x) = -\frac{C^3}{q\epsilon}(dC/dV)^{-1}. \tag{4}$$

Kennedy and O'Brien (KOB) [3] point out that if (4) is indeed correct, then the true doping profile can be obtained from the $C-V$ data by using (4) and then applying the following formula:

$$N(x) = n_0(x) - \left(\frac{kT}{q}\right)\left(\frac{\epsilon}{q}\right)\frac{d}{dx}\left[\frac{1}{n_0(x)}\frac{d}{dx}n_0(x)\right]. \tag{5}$$

The successful use of (5), however, rests on the accuracy of (4). In their arguments regarding (4), KMK used the full and accurate formulation for $n_0(x)$, but in expressing the free carrier distribution for biased conditions they made the approximation of an edge in $n(x)$ such that, in the present notation, $n(x)=0$ for $0<x<w$ and $n(x)=n_0(x)$ for $x>w$, thus essentially assuming a zero value of Debye length at this stage of the calculations. In the KMK approximation, an increment of voltage causes a quantity of mobile electrons equal to $n_0(w)\Delta w$ to circulate through the external circuit, thus sampling $n_0(x)$ at $x=w$ and leading to (4).

The accuracy of (4) must be determined before the range of validity of (5) can be evaluated. A general solution of the problem seems out of the question. Carter [4] and Carter, Gummel, and Chawla [5] have reported the results of computer studies of Gaussian profiles which show that expression (4) is not precise, although for the profiles analyzed it provided good approximations. The present paper investigates these matters further.

V. Results of Computer Simulations

This section presents the results of a computer study (see the Appendix) which was designed to show the relationship between the true doping profile of a semiconductor and the conclusions regarding that profile which can be deduced from externally measured $C-V$ data. Two types of profiles were used in this study: step functions, which should impose the most stringent tests on the relationships, and linear ramps to show the effects of finite gradients. For each assumed doping profile, a set of bias voltages was assumed, and for each of these an iterative procedure was used to compute the majority-carrier distribution $n(x)$ and the distributed increment of majority carriers $\Delta n(x)$ that would be produced by an increment in voltage ΔV. From the results of these calculations the $C-V$ relationship corresponding to the assumed $N(x)$ was computed. The calculated $C-V$ relationship was then used in the formulas designed for the determination of $N(x)$ from such data, and the results were compared with the known doping profile.

In presenting the results of the computer simulation we shall define an "apparent doping profile," $N^*(x)$, which is the result of substituting the $C-V$ relationship into the conventional formula (1), i.e.,

$$N^*(x) = -\frac{C^3}{q\epsilon}(dC/dV)^{-1} \tag{6}$$

where

$$x = \epsilon/C. \tag{7}$$

In the conventional depletion-layer approximation we would have $N^*(x)=N(x)$. In the KMK approximation, $N^*(x)=n_0(x)$.

We shall also define a "second estimate," $N^{**}(x)$, by an equation analogous to the KOB formula (5) in order to determine the effect of the KOB correction when applied to the KMK approximation:

$$N^{**}(x) = N^*(x) - \left(\frac{kT}{q}\right)\left(\frac{\epsilon}{q}\right)\frac{d}{dx}\left[\frac{1}{N^*(x)}\frac{d}{dx}N^*(x)\right]. \tag{8}$$

In the KMK approximation we would have $N^{**}(x)=N(x)$.

The results of the calculations are presented in normalized form. Normalization of doping intensities and of majority-carrier densities is done with respect to the intensity of doping on the high side; i.e., using the subscript n to denote *normalized:*

$$N_n = \frac{N}{N_{\text{high}}}$$

$$n_n = \frac{n}{N_{\text{high}}}$$

and

$$n_{n0} = \frac{n_0}{N_{\text{high}}}.$$

Distance are normalized with respect to the Debye length on the high side of the doping profile:

$$x_n = \frac{x}{\lambda_{\text{high}}}$$

where

$$\lambda_{\text{high}} = \sqrt{\frac{kT\epsilon}{q^2 N_{\text{high}}}}.$$

Voltages are normalized with respect to kT/q:

$$V_n = \frac{V}{kT/q}.$$

The normalized results of the computations are presented in Figs. 3 through 13. They can be divided conveniently into the four categories labeled A through D below.

A. Majority-Carrier Distributions

Fig. 3 contrasts the distributions of majority carriers when depletion is done from contacts placed on the low and high sides of the doping profile, respectively. In these examples the doping profile is a step with a high–low ratio of 10:1. Shown in Fig. 3(a) are the normalized $n_0(x)$ and the normalized majority-carrier distributions for various values of voltage, identified by the labels, applied to a contact located on the low side of the profile at $x_n = -30$. Fig. 3(b) is drawn for the same doping profile but with the contact located on the high side at $x_n = 6\sqrt{10}$. It can be seen 1) that the majority-carrier distributions do not have sharp edges but instead require several Debye lengths to make the transition from approximate depletion to approximate space-charge neutrality; 2) that an increment in voltage does not provide a sample of either $N_n(x)$ or $n_{n0}(x)$; and 3) that the results depend on the side from which depletion is done.

B. Comparisons Among $N^*(x)$, $N(x)$, and $n_0(x)$

Figs. 4 through 8 compare the apparent doping profile deduced conventionally from C–V data, i.e., $N^*(x)$ as defined by (6), with the true profile $N(x)$ and the majority-carrier distribution with contacts far away, $n_0(x)$.

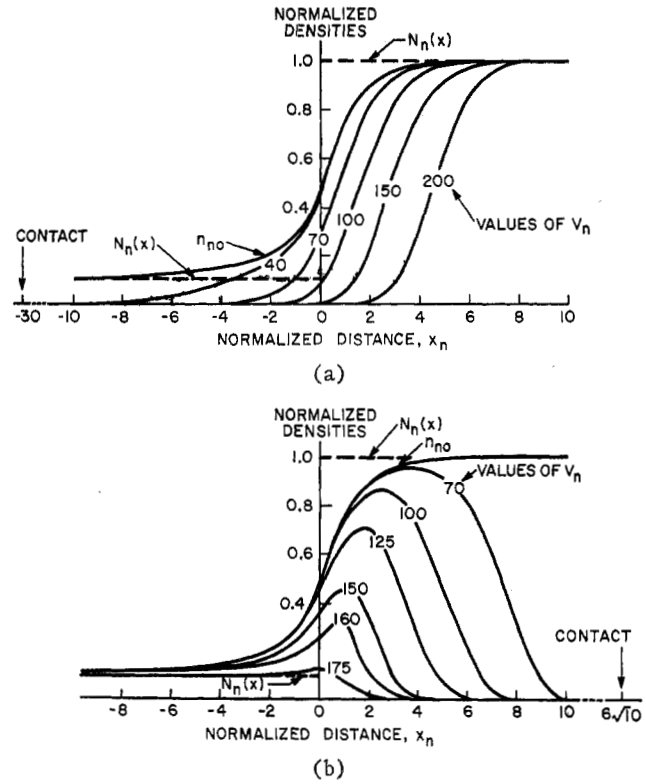

Fig. 3. A set of majority-carrier distributions for a step profile with a high–low ratio of 10:1, for various values of bias voltage applied to a contact on the (a) low side, (b) high side.

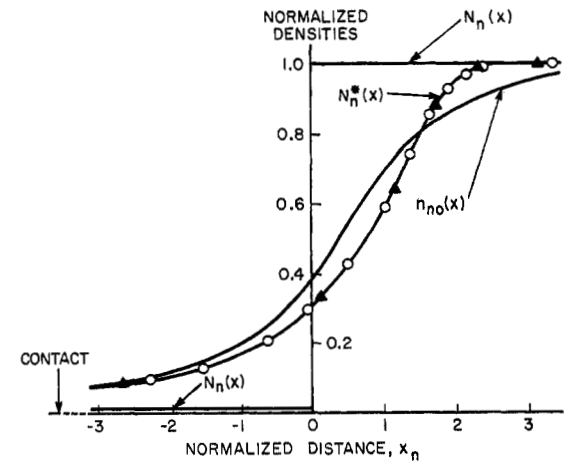

Fig. 4. Comparison among $N(x)$, $n_0(x)$, and $N^*(x)$ for a step profile with a high–low ratio of 100:1 and with depletion from the low side.

Fig. 4 is drawn for a step profile with a high-low ratio of 100:1 and with depletion done from the low side.[1] It can be seen that the discrepancy between $N^*(x)$ and $N(x)$ will be clearly visible if spatial resolution is attempted to better than several Debye lengths. Also,

[1] The points on $N^*(x)$ shown by the solid triangles were computed by D. L. Scharfetter, using a different computer program, to provide us with an independent check on the present results.

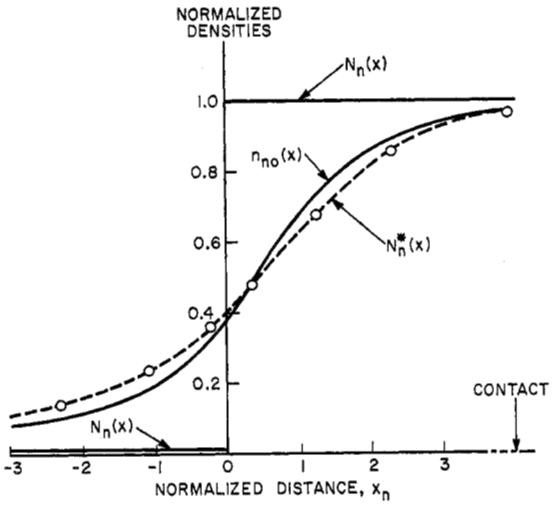

Fig. 5. Similar to Fig. 4, but with depletion from the high side.

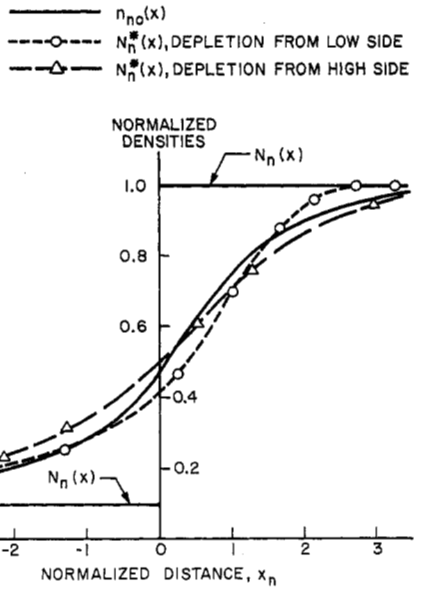

Fig. 6. Similar to Figs. 4 and 5, but for a step profile with a high–low ratio of 10:1.

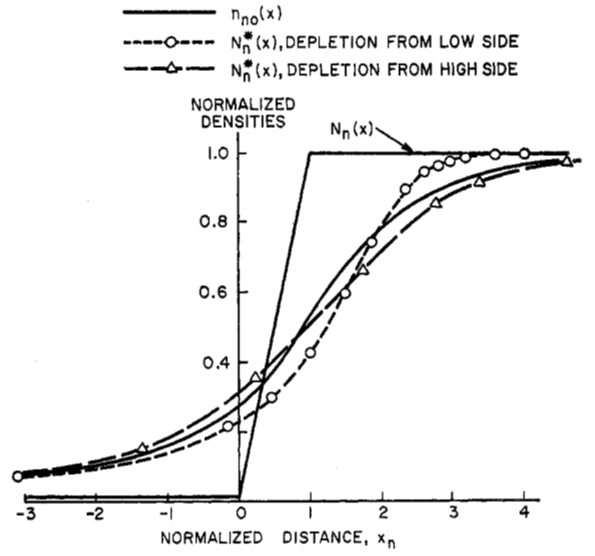

Fig. 7. For a linear ramp with a width equal to λ_{high} connecting uniform sections with a high–low ratio of 100:1.

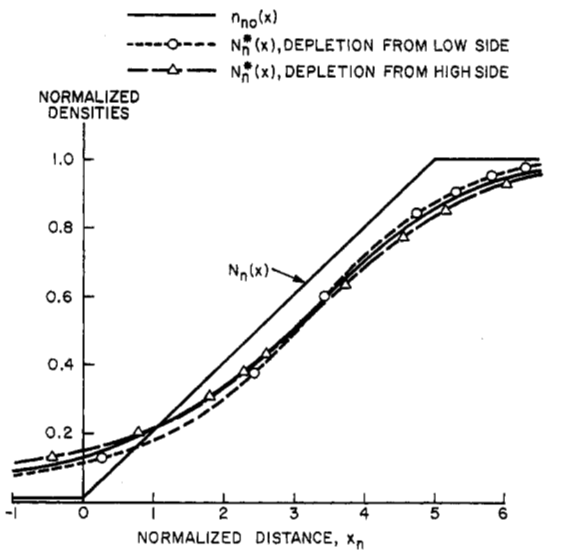

Fig. 8. For a linear ramp with a width equal to $5\lambda_{high}$ connecting uniform sections with a high–low ratio of 100:1.

$N^*(x)$ is appreciably different from $n_0(x)$. Fig. 5 is similar to Fig. 4 except that here depletion is done from the high side. The apparent doping profile, $N^*(x)$ as obtained from (6), is not quite as good an approximation to $N(x)$ as it was in Fig. 4, but it is a better approximation to $n_0(x)$.

Fig. 6 is like Figs. 4 and 5 except that it is drawn for a step profile with a high–low ratio of 10:1. Here the two functions $N^*(x)$ are not quite so much different for depletion from opposite sides, but, within a spatial resolution of several Debye lengths, neither provides a good approximation to $N(x)$. Inasmuch as the differential-capacitance method provides a correct measure of doping density regardless of Debye length when the doping is uniform, smaller discrepancies are to be expected as the step ratio is diminished.

Fig. 7 shows the results obtained for a profile which consists of a linear ramp of width equal to λ_{high} which joins two uniformly doped sections with a high–low ratio of 100:1. The results are barely distinguishable from those of the step profile presented in Figs. 4 and 5.

In Fig. 8 the linear ramp has a width equal to $5\lambda_{high}$, and the high–low ratio is again 100:1. Here the results are approximately the same for depletion from either side. Over most of the ramp section, either of the functions $N^*(x)$ represents $N(x)$ to within a spacial accuracy

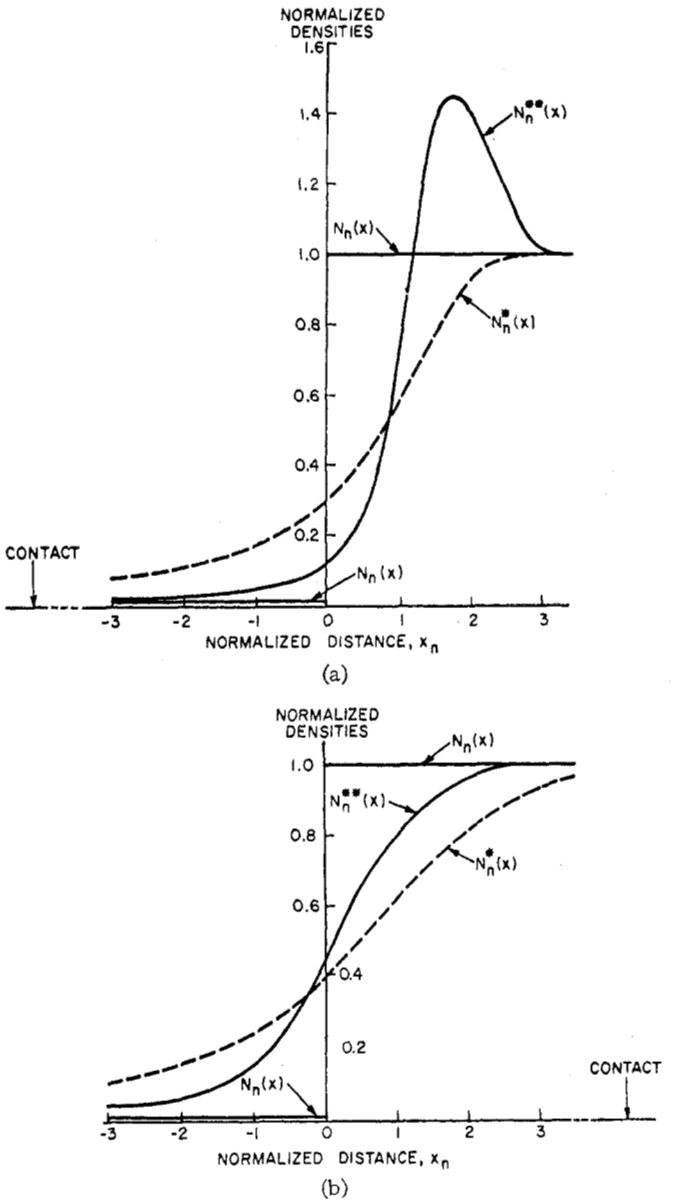

Fig. 9. Comparison among $N(x)$, $N^*(x)$, and $N^{**}(x)$ for a step profile with a high–low ratio of 100:1 and with depletion from (a) low side, (b) high side.

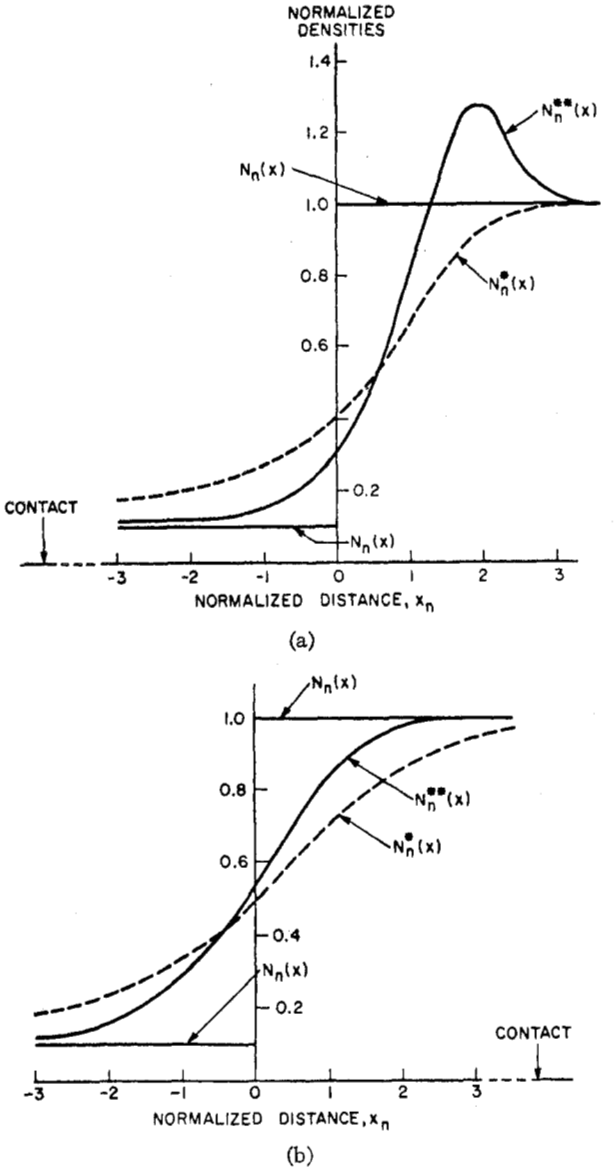

Fig. 10. Similar to Fig. 9, but drawn for a step profile with a high–low ratio of 10:1. Depletion is from (a) low side, (b) high side.

of about $0.5\lambda_{high}$. Throughout the whole range, both functions $N^*(x)$ are quite close to $n_0(x)$, in the manner proposed by KMK.

C. Comparisons Among $N^*(x)$, $N^{**}(x)$, and $N(x)$

KOB showed that, if $n_0(x)$ were known, (5) could be used to determine $N(x)$. In the actual situation, however, we do not know $n_0(x)$, but from C–V measurements we can determine $N^*(x)$ by use of (6). Thereupon we can use (8) to compute the second estimate, $N^{**}(x)$. As we have seen, $N^*(x)$ is not identical with $n_0(x)$, and so $N^{**}(x)$ will not in general be identical with $N(x)$. Figs. 9 through 11 compare the two estimates, $N^*(x)$ and $N^{**}(x)$, with $N(x)$ for the various profiles previously examined in Figs. 4 through 8.

Fig. 9(a) is drawn for a 100:1 step with depletion from the low side and corresponds to Fig. 4. It can be seen in Fig. 4 that $N^*(x)$ has a much greater curvature than $n_0(x)$ in the vicinity of $x_n = 2$. Formula (8) requires two derivatives, and the result, as shown in Fig. 9(a), is a large overcorrection in $N^{**}(x)$ near $x_n = 2$. Here the function $N^{**}(x)$ might well be regarded as a poorer estimate of $N(x)$ than was provided by $N^*(x)$ itself.

Fig. 9(b) is drawn for a 100:1 step with depletion from the high side. This corresponds to Fig. 5 where it was seen that capacitance measurements made with depletion from the high side provide a function $N^*(x)$ that is a somewhat better approximation to $n_0(x)$ than would be obtained with depletion from the low side. Particularly, the excessive curvature near $x_n = 2$ is missing. In consequence, $N^{**}(x)$ in Fig. 9(b) is a better

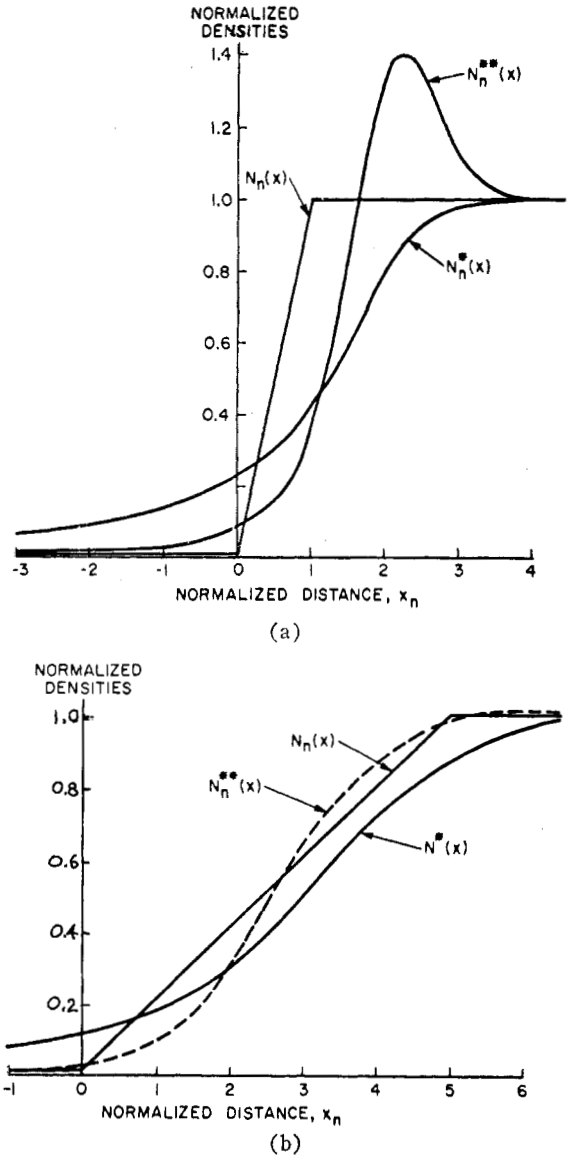

Fig. 11. Comparison among $N(x)$, $N^*(x)$, and $N^{**}(x)$ for ramps of widths (a) λ_{high}, (b) $5\lambda_{high}$ that join uniform sections with a high–low ratio of 100:1. Depletion is from the low side.

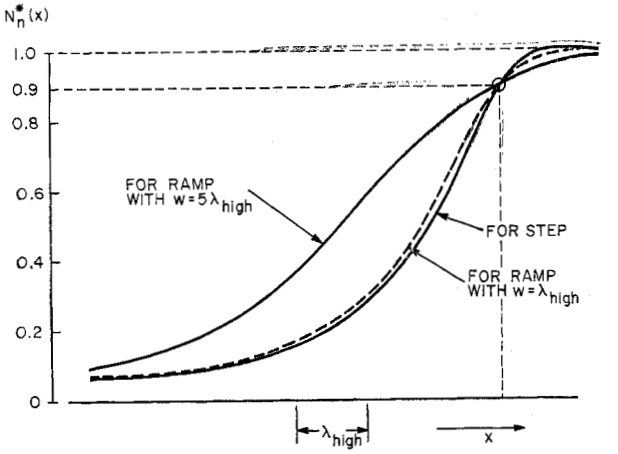

Fig. 12. Comparison among the apparent doping profiles, $N^*(x)$, as they would be deduced from $C-V$ data, for three doping profiles: a step and two ramps. The high–low ratio is 100:1. Depletion is from the low side.

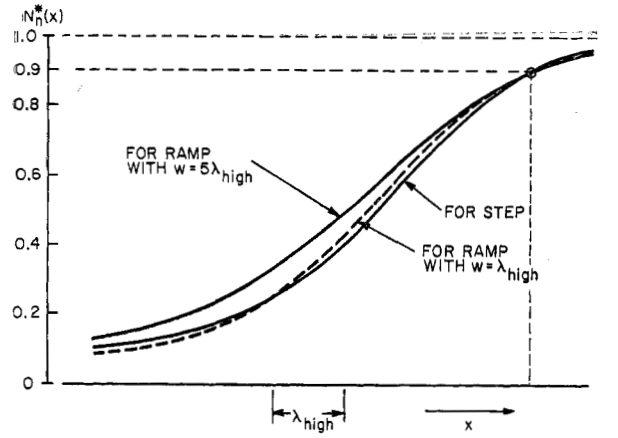

Fig. 13. Similar to Fig. 12, but with depletion from the high side.

estimate of $N(x)$ than was provided by $N^*(x)$ itself. The differences, however, will be clearly visible if spatial resolution is attempted to better than one or two Debye lengths.

Fig. 10 is drawn for a 10:1 step. The results are similar to those for the 100:1 step. The smaller step produces a smaller overshoot in the low-side $N^{**}(x)$, as might be expected.

Fig. 11(a) shows the results for a linear ramp of width equal to λ_{high} which joins uniform sections with a high–low ratio of 100:1. Depletion is from the low side. The results are very similar to those of Fig. 9(a) for a 100:1 step.

Fig. 11(b) is drawn for a ramp with a width equal to $5\lambda_{high}$. Depletion is from the low side. $N^{**}(x)$ is a better estimate of $N(x)$ than is provided by $N^*(x)$. The overshoot of $N^{**}(x)$ to the right of the ramp is inappreciable. Spacial resolution on the order of a Debye length is feasible.

D. Comparison of the Functions $N^*(x)$ for the Various Doping Profiles

In order to illustrate the practical difficulties inherent in the attempted measurement of doping profiles with large gradients by the differential-capacitance technique, Figs. 12 and 13 show capacitance-deduced apparent doping profiles $N^*(x)$ for the 100:1 step and for the two ramps with $w=\lambda_{high}$ and $w=5\lambda_{high}$. For ease of comparison, these curves are plotted so that their 90 percent points coincide. In a practical situation these curves would be derived from experimental data, and any two curves that cannot be distinguished from each other do not contain sufficient information to distinguish between the two doping profiles that produced them. We see that if we allow for only a little experimental error, the graphs of $N^*(x)$ for the step and for the ramp

with $w=\lambda_{high}$ are essentially indistinguishable. It appears that the function $N^*(x)$ is so insensitive to the details of a change that occurs in one Debye length or less that the information regarding the exact profile is essentially lost. The situation is somewhat better for the ramp that makes the transition from low to high in five Debye lengths.

VI. Summary and Conclusions

We have shown the results of a computer simulation of the differential-capacitance technique that has been carried through for semiconductors with one-sided step and ramp doping profiles. The object has been to study the accuracy of the estimates of doping profiles that can be made from $C-V$ data.

It is shown that an increment in applied voltage produces an increment in majority-carrier distribution that is not localized as is assumed in the simple theory but which is distributed over several Debye lengths. Consequently, the apparent doping profile obtained from the $C-V$ measurements, i.e., $N^*(x)$ as defined by (6), is somewhat different from the actual doping profile $N(x)$. The discrepancy can be phrased in terms of the spatial resolution of the profile expressed in Debye lengths corresponding to the doping on the high side of the profile.

For step profiles, the differences between $N^*(x)$ and $N(x)$ become evident if spatial resolution is attempted to less than a few Debye lengths. The high–low ratio of the step is not of great significance in the resolution achieved. The apparent doping profile is somewhat different if depletion is done from a contact placed on the high side of the profile than if depletion is done from the low side.

For a linear ramp that joins uniformly doped high and low sections, the results depend on the width of the ramp. For a ramp with a width of one Debye length, the results obtained from $C-V$ measurements can hardly be distinguished from those of an abrupt step. With a width of five Debye lengths, the spatial resolution of the profile is of the order of a Debye length and the ramp can therefore be distinguished from a step.

The results of the computations also show that the apparent doping profile, $N^*(x)$, is a somewhat closer representation of the majority-carrier distribution with contacts far away, $n_0(x)$, than it is of the doping profile itself, but the two functions are not identical. The discrepancy between $N^*(x)$ and $n_0(x)$ becomes smaller with shallower ramps, and for a ramp with a width of five Debye lengths the two functions are quite close to each other.

Also compared in this paper are the results of a second estimate of $N(x)$, i.e., $N^{**}(x)$ as defined by (8), which is predicated on a close representation of $n_0(x)$ by $N^*(x)$. Either for a step or for a ramp with a width of one Debye length, and for depletion from the low side, the function $N^{**}(x)$ shows a large overshoot on the high side of the profile. If depletion is done from the high side, $N^{**}(x)$ provides a slightly improved estimate of $N(x)$. For a ramp with a width of five Debye lengths, $N^{**}(x)$ provides an improved estimate of $N(x)$ even with depletion from the low side, but the spatial resolution of the profile is still of the order of a Debye length. Depletion from the high side improves the accuracy somewhat, but it will be recognized that the two derivatives required in applying (8) will greatly reduce the practical value of attempting the correction.

In brief, the results of the present study of semiconductors with high–low profiles indicate that $C-V$ data are insensitive to changes in the doping profile that occur in a distance that is smaller than the Debye length corresponding to the doping on the high side, and that profiles determined by the $C-V$ method should be expected to provide a spatial resolution only of the order of a Debye length.

Appendix

We neglect the contribution of minority carriers to space charge and write Poisson's equation as

$$\frac{dE}{dx} = \frac{q}{\epsilon}[n(x) - N(x)] \tag{9}$$

where E is the electric field intensity defined with positive direction opposite to positive x, $n(x)$ is the density of majority carriers, and $N(x)$ is the net density of ionized impurity atoms. Current in the reverse-biased junction is assumed to be essentially zero, and so

$$J_x = q\left(D\frac{dn}{dx} - \mu n E\right) = 0. \tag{10}$$

In solving these equations it is useful to introduce the potential ψ, given by

$$E = -\frac{d\psi}{dx}. \tag{11}$$

From this and the Einstein relation $D/\mu = kT/q$ we can reduce (10) to

$$n = \nu_0 e^{-q\psi/kT} \tag{12}$$

where ν_0 is the value of $n(x)$ at the position where ψ is taken to be zero. We shall place $\psi = 0$ deep in the body of the semiconductor, and so $\nu_0 = N(\infty)$, where $N(\infty)$ is the intensity of doping as $x \to \infty$.

The substitution of (11) and (12) with $\nu_0 = N(\infty)$ into (9) yields the relation

$$\frac{d^2\psi}{dx^2} = \frac{q}{\epsilon}[N(x) - N(\infty)e^{-q\psi/kT}]. \tag{13}$$

This is to be solved subject to the boundary conditions that $\psi(\infty) = 0$ and $\psi(0) = V$, where V is the sum of the built-in and applied reverse-bias voltages. In solving (13) numerically, it is expedient to start the solution with a given value of V and an assumed value of $E(0) = -(d\psi/dx)_0$ and iterate through an appropriate series

of values of $E(0)$ until the boundary condition $\psi(\infty)=0$ is satisfied to a satisfactory degree of accuracy.

The capacitance C was determined by solving (13) for two applied voltages which differ by a small increment ΔV. The increment of charge is given by

$$\begin{aligned}\Delta Q &= -\int_0^\infty q[n_2(x) - n_1(x)]dx \\ &= \epsilon[E_2(0) - E_1(0)] \\ &= \epsilon\Delta E(0)\end{aligned}$$

where the subscripts 1 and 2 refer to the values for the first and second applied voltages, respectively. The capacitance is given by

$$C = \frac{\Delta Q}{\Delta V} = \epsilon\frac{\Delta E(0)}{\Delta V}. \tag{14}$$

Equations (6) and (8) were then used to obtain the apparent and "corrected" doping profiles, $N^*(x)$ and $N^{**}(x)$.

Acknowledgment

The authors wish to thank G. E. Smith for his contributions to basic aspects of this study; D. L. Scharfetter for computing the independent check points of Fig. 4; B. R. Chawla and W. E. Carter for providing additional confirming computations; and H. J. Boll, H. K. Gummel, W. S. Johnson, W. T. Lynch, B. T. Murphy, and R. J. Strain for their helpful discussions of the problem.

References

[1] J. Hilibrand and R. D. Gold, "Determination of the impurity distribution in junction diodes from capacitance-voltage measurements," *RCA Rev.*, vol. 21, June 1960, pp. 245–252.
[2] D. P. Kennedy, P. C. Murley, and W. Kleinfelder, "On the measurement of impurity atom distributions in silicon by the differential capacitance technique," *IBM J. Res. Develop.*, Sept. 1968, pp. 399–409.
[3] D. P. Kennedy and R. R. O'Brien, "On the measurement of impurity atom distributions by the differential capacitance technique," *IBM J. Res. Develop.*, Mar. 1969, pp. 212–214.
[4] W. E. Carter, private communication.
[5] W. E. Carter, H. K. Gummel, and B. R. Chawla, "Interpretation of capacitance vs. voltage measurements of p-n junctions," to be published.

Correspondence

Thermal Resistance Measurement of Avalanche Diodes

***Abstract*—A new method of thermal resistance measurement is presented. The variation of diode breakdown voltage with input power as a function of time is the basis of the method. Diode space-charge resistance and series resistance together with separate components of heat-flow resistance are measured using this method. The technique of the measurement is straightforward and provides results with little ambiguity and high accuracy.**

Introduction

The extreme power densities of current avalanche diodes require careful consideration of the heat-flow properties of these devices in a useful circuit environment. Of great importance is the method of heat-flow measurement. This measurement should portray all of the intricacies of heat flow from the diode junction through the diode-package interface into the heat sink.

A number of techniques exist for the measurement of heat-flow resistance [1], [2]. Of these, the most valuable are those which use the temperature dependence of the breakdown voltage [2]. This approach not only affords a convenient indication of junction temperature, but also allows heat-flow measurements in the actual operating mode of the diode.

Fig. 1 shows a reverse voltage–current characteristic of an avalanche diode. The finite resistance of the reverse characteristic is largely due to the temperature dependence of breakdown voltage. An incremental increase in current I_B causes an incremental power increase with an attendant increase in junction temperature. The junction temperature increase, in turn, causes an incremental rise $\Delta V_B(T)$ in breakdown voltage. The resistance thus derived is referred

Manuscript received October 7, 1970; revised April 28, 1971.

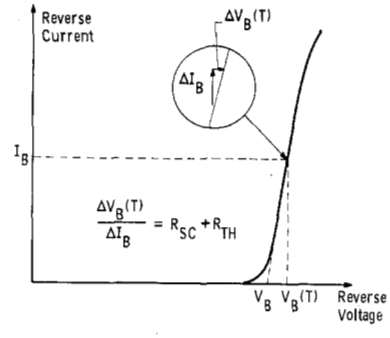

Fig. 1. Reverse voltage–current characteristic of an avalanche diode.

to as the thermal resistance of the diode [2]. Measurement of the thermal resistance leads directly to the heat-flow resistance by the equation [3] $R_{TH} \approx r\beta V_B^2$, where r is the heat-flow resistance[1] and β the temperature coefficient of V_B, $\beta V_B = \Delta V_B/\Delta T$. If V_B and β are known, r may be calculated.

There are several complications in the determination of the thermal resistance. The incremental slope of the curve in Fig. 1 has resistive components other than thermal. One is the spreading resistance of the diode and the other is the space-charge resistance. In nearly all cases for avalanche diodes the spreading resistance is negligible. The space-charge resistance may or may not be negligible. Its contribution to the total incremental resistance should be measured.[2]

[1] $r = (T_i - T_0/V_B I_B)$; where T_i = junction temperature, T_0 = heat sink temperature.
[2] The test of poorer diodes shows a contact resistance which further complicates this measurement.